ELSEVIER

Coastal Engineering 37 (1999) 431–453

COASTAL ENGINEERING

www.elsevier.com/locate/coastaleng

Monitoring surface waves in coastal waters by integrating HF radar measurement and modelling

Cees de Valk [a,*], Ad Reniers [b,1], John Atanga [c], Ascension Vizinho [c,2], Jur Vogelzang [d,3]

[a] *ARGOSS, P.O. Box 61, 8325 ZH Vollenhove, Netherlands*
[b] *WL|Delft Hydraulics and NCK, Delft University of Technology, Netherlands*
[c] *University of Sheffield, UK*
[d] *National Institute for Coastal and Marine Management / RIKZ, UK*

Abstract

A new scheme for retrieval of wave spectra in coastal seas from HF radar data has been developed which is capable of measuring directional wave spectra even from the data of the single antenna array. It does this by making use of a wave propagation model to link wave spectra, and therefore also HF radar Doppler spectra at different points in space. The resulting scheme processes all HF radar data within the area covered by the system simultaneously. In coastal applications, the method offers increased flexibility in the radar configuration and improved coverage. Tests are reported on simulated HF radar data, and a first application to HF radar data collected near Holderness on the English east coast is reported.

Keywords: Sea surface waves; Measurement; Modelling; HF radar; Inversion

1. Introduction

Shore-based HF radar systems have proven capable of measuring directional spectra of sea surface waves in coastal seas, as shown in this issue by Wyatt et al. (1998). The underlying physical principles were developed years ago by Barrick (1972a,b). Basi-

* Corresponding author. Fax: +31-527-242016; E-mail: valk@argoss.nl
[1] Fax: +31-15-2858582; E-mail: reniers@wldelft.nl.
[2] Fax: +44-114-222-3809; E-mail: j.atanga@sheffield.ac.uk.
[3] Presently at Rijkswaterstaat, Survey Department. Fax: +31-15-2618962; E-mail: j.vogelzang@mdi.rws.minvenw.nl.

0378-3839/99/$ - see front matter
PII: S0378-3839(99)00037-X

cally, the radar backscatter is related to ocean waves of half the wavelength of the radio signal which propagate toward or away from the antenna; the mechanism is that of Bragg scattering. The backscattered signal can be used to determine the direction of short wind-waves as well as the current, which causes an additional Doppler shift in the frequency of the returned signal. However, the same interactions between waves which cause them to deviate from a sinusoidal shape also lead to secondary peaks in the Doppler spectrum of the HF radar return signal; see Fig. 1 for examples. These peaks are strongly related to the shape of the directional wave spectrum over a wide range of frequencies and propagation directions.

Recently, these principles were successfully applied to obtain continuous and detailed measurements of directional wave spectra near Holderness on the east coast of England by Wyatt (1997, 1998) and Wyatt et al. (1998), using data collected by the OSCR HF radar of Fugro GEOS. To retrieve sea surface wave spectra from HF radar Doppler spectra, the mapping from wave spectrum to Doppler spectrum was inverted according to an algorithm introduced by Wyatt (1990). This algorithm is applied to the Doppler spectra from two suitably located antenna arrays representative of a single *cell*, which is a patch of sea surface resolved by the radar. Because the two antenna arrays view the sea surface waves from different angles, information about the propagation directions of the waves can be obtained. Processing the data cell-by-cell then leads to a synoptic picture of the wave spectrum as it varies within the area covered by the radar system. Other methods which have been proposed also retrieve the wave spectrum cell-by-cell and differ only in the inversion technique employed (Howell and Walsh, 1993; Hisaki, 1996).

Attractive as cell-by-cell inversion may be, there may be situations in which retrieval of wave spectra from the HF radar data is difficult. Wave spectra can only be retrieved in those cells for which the signal-to-noise ratio at *both* antennae is high enough. If the

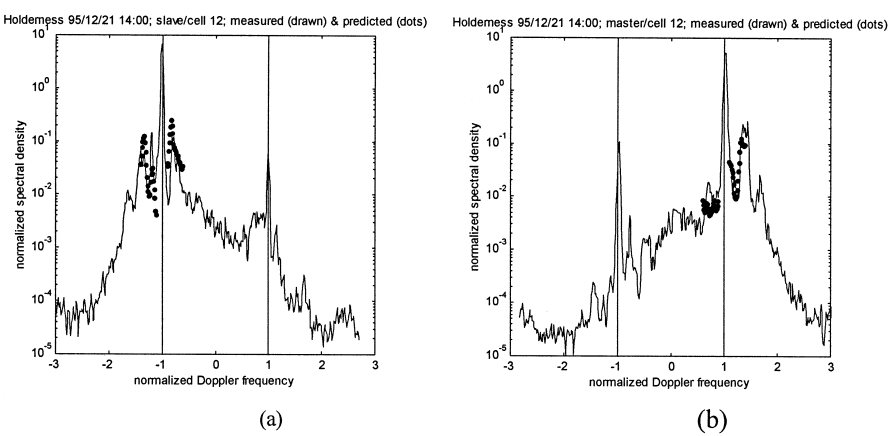

Fig. 1. Example of Doppler spectra measured by slave (a) and master (b) antenna (drawn line), and predicted spectra matched to data from the slave (a) and master (b) antenna (dots). The spectra and frequencies are normalised; Doppler shifts due to current have been removed.

antenna positions are chosen to optimise wave measurement, normally the signal-to-noise ratio is sufficient in a restricted area. However, in practice, the antenna positions are often not optimal for wave measurement (Ledgard and Wyatt, 1997). The main objective of most HF radar campaigns is current measurement, which poses different requirements on antenna configuration than wave measurement does. Moreover, it is often not easy to find suitable sites to deploy the equipment because of access restrictions, coastal topography and logistic problems. For these reasons, an alternative to the two-antenna cell-by-cell retrieval method was developed within the SCAWVEX project with the objective of reducing the sensitivity to antenna configuration and to noise.

On deep water, often currents and wave spectra vary on length scales beyond the radar range of typically 20–50 km and on time-scales beyond the integration time of the radar of typically 15–30 min. When measuring from a platform in such an area, the directional wave spectrum can be obtained using only a single antenna array. In this case, waves from the same ensemble are present in different cells viewed under different azimuth angles, so the data from these cells can be combined straightforwardly.

This simple idea cannot be applied near the coast. Here, wave conditions vary due to fetch-limited wave growth and to shallow-water wave transformations such as refraction, shoaling and dissipation. However, most of these processes are fairly well understood, so this knowledge might be used together with the HF radar Doppler spectra from different cells to estimate simultaneously the directional wave spectra within a certain region. A wave component with a certain initial propagation direction and period approaching the shore can be observed by a single antenna in different cells along its path and (generally) from different angles. These observations, combined with a simple

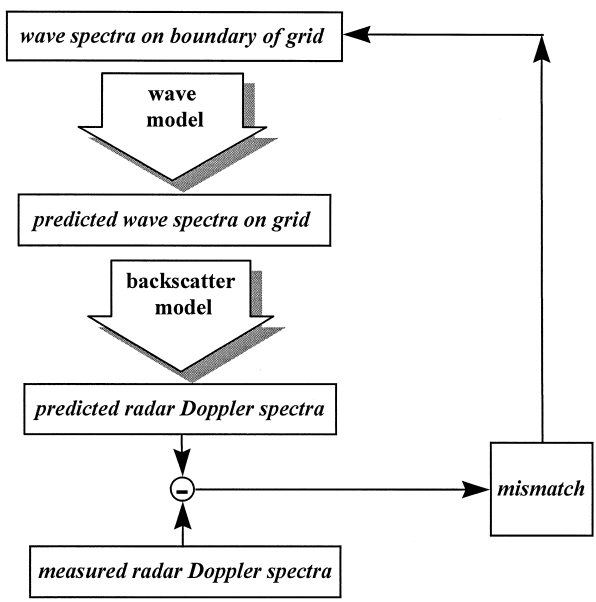

Fig. 2. Overview of the coupled retrieval method.

model predicting its path and change in direction, may therefore be sufficient to identify the amplitude of this particular wave component. This paper presents a new scheme for retrieval of sea surface wave spectra from HF radar data which imposes physical constraints onto the estimates, and describes tests aimed to find out whether it allows us to relax restrictions on antenna configuration and even work with a single antenna array only. These tests comprise simulations as well as applications to HF radar data from the above mentioned Holderness campaign.

Fig. 2 summarises the mechanism employed to incorporate wave model constraints into the retrieval of wave spectra from HF radar Doppler spectra. A wave model needs certain input data, for example wave spectra at the boundary of the model grid. Everywhere within its grid, it computes wave spectra which are fed into a radar backscatter model to predict the Doppler spectra measured by the HF radar system. Normally, the predicted spectra will not match the measured spectra exactly. The degree of mismatch is expressed in terms of a scalar measure to be discussed later, and the boundary conditions of the wave model are adjusted step-by-step to attain the smallest mismatch possible.

The models will be discussed in the Section 2, Section 3 deals with the retrieval method and its tests on simulated data, and Section 4 with the application to data from the Holderness experiment.

2. Models

2.1. Shallow-water wave transformations

Sea surface waves can be described statistically in terms of the variance density spectrum S as a function of the wavenumber vector $\boldsymbol{k}$, or alternatively, in a static frame of reference, as a function of frequency ω and propagation direction θ. ω is related to the wavenumber by the dispersion relation and a Doppler shift:

$$\omega = \sigma + \boldsymbol{k} \cdot u \tag{1a}$$

$$\sigma^2 = gk \tanh(kd) \tag{1b}$$

with u as the current, d the water depth, σ the intrinsic frequency (in a moving frame of reference) and $k = |\boldsymbol{k}|$. The evolution of sea surface waves is most conveniently described in terms of the action density

$$N = S/\sigma \tag{2}$$

and follows from the balance equation (e.g., Komen et al., 1994), which in the steady case (with steady current and depth) reads

$$\nabla_x \cdot (c_g + u) N + \nabla_\theta \cdot (v_\theta N) = Q \tag{3}$$

In Eq. (3), c_g is the group velocity, v_θ is the rate of change of the angle of propagation and Q is the sum of all sources and sinks of action (dissipation, wind forcing,

wave–wave interactions). The solution of Eq. (3) for a strip of coastal sea depends on imposed action densities for incoming waves along the wet part of the boundary (which is not a coastline) and on the local wind field.

For a limited area reached by HF radar systems such as OSCR and WERA, the steady approximation (Eq. (3)) is reasonably accurate. For example, a packet of 100 m waves will take only about 1.5 h to travel over a distance of 25 km on water of 10 m depth. Offshore wave conditions normally vary on time-scales between 1 and 3 h; see, e.g., the time-series in the work of Wyatt et al. (1998). In fact, in routine wave monitoring spectra are often estimated with an interval of 3 h. So considering the wave spectra in a limited area of coastal sea as a fixed function of the boundary conditions and forcing does not seem unreasonable. The approximation simplifies the problem of retrieval of wave spectra from HF radar drastically. Once a method for the steady situation is developed, it may be extended in the future to deal with the non-steady case as well.

Wave propagation (represented by the left-hand side of Eq. (3)) involves propagation in the plane, shoaling (increase in action density resulting from the deceleration of waves in shoaling depths) and refraction (bending of wave rays caused by depth or current variation, see, e.g., Mei, 1989). In the present study, currents were neglected although the wave model could take them into account. In fact, the current field could be estimated from HF radar data and inserted into the wave model. The omission of currents in the present study is expected to affect mainly simulations of shorter waves, which are more sensitive to currents. Our tests were carried out in a region where wave–current interaction is not extremely strong (Section 4). Nevertheless, the topic deserves to be addressed in a future study.

The source term Q in Eq. (3) was strongly simplified in comparison with, e.g., the WAM model (Komen et al., 1994) or its adaptation to shallow water SWAN (Booij et al., 1996). Within a coastal strip of the order of 25 km wide, long wind sea or swell waves coming in through the offshore boundary normally dominate over locally generated waves, unless coastal waters are sheltered by islands or shoals. The exceptions are situations with wind blowing offshore which are not of much practical interest for coastal engineering applications. When long waves from open sea dominate, generally dissipation by bottom friction or breaking are the most important source terms. Growth of these waves in a restricted area is very limited. The same holds for whitecapping and four-wave interactions, which are of the same order of magnitude. In the model of this study, only one source term was included, which is bottom friction. It was represented by the simple JONSWAP relationship which has one empirically determined constant from (Komen et al., 1994). In view of the highly approximate nature of the JONSWAP relationship, we could leave this constant unspecified and estimate it from the HF radar data, but this has not been done so far.

The balance Eq. (3) was solved by marching the solution from an offshore boundary toward the shore, using a first-order octant upwind scheme for the transport of action in the along-shore coordinate and in the propagation direction (see Petit, 1995). The (linear) bottom friction source term was integrated implicitly. Boundary conditions were imposed explicitly only along the offshore boundary. Along the open side boundaries of the grid, the along-shore gradient of the action density was assumed to vanish, so spectra

on this part of the boundary were copied from the nearest interior grid line after propagating them. Propagation directions were restricted to angles within $\pm 72^\circ$ about the cross-shore grid axis. This implies that no spectral densities were computed outside this sector so these are fixed to zero. This simple approach only works with a relatively straight coastline and simple bathymetry, i.e., where propagation is almost a one-dimensional problem. In more complex areas, a more flexible propagation scheme such as implemented in SWAN should be used (Booij et al., 1996).

The only input data required by the wave model just described are the action density spectra at all grid-points along the offshore boundary. These are therefore the variables to be retrieved from the HF radar data (see Section 3.1 and following). Typically, specification of these boundary conditions requires $n_\theta \times n_\omega \times n_y$ numbers, with n_θ the number of propagation directions (typically 12), n_ω the number of frequencies (typically 25), and n_y the number of grid points along the offshore boundary (17 in the application described in Section 4). A typical array size for the boundary conditions is therefore 5000. Clearly, these numbers cannot be independent: wave spectra on deep water are correlated in space and there should be some coherence in the spectral domain as well.

The boundary spectrum at a single gridpoint was described in terms of the logarithm of the action density (see Section 2.1), so the action density itself is guaranteed to be nonnegative. Writing $N^0(\omega,\theta,y)$ for the action density on the offshore boundary as a function of frequency, propagation direction and alongshore coordinate, it was represented as

$$\log N^0(\omega,\theta,y) = \sum_{\substack{i_\omega=1,\ldots,n_\omega \\ i_\theta=1,\ldots,n_\theta \\ i_y=1,\ldots,n_y}} \left[\alpha^{l}_{i_\omega,i_\theta,i_y} \cos\big(\theta\kappa(i_\theta-1)\big) + \alpha^{ll}_{i_\omega,i_\theta,i_y} \sin\big(\theta\kappa(i_\theta-1)\big) \right] \times B_{i_\omega}(\log(\omega))\, B_{i_y}(y) \tag{4a}$$

with

$$\kappa = \tfrac{2}{3}\pi/\Delta\theta \tag{4b}$$

and $\Delta\theta$ the width of the interval of propagation directions in the model. The frequency-dependence was represented by B-splines $B_1, B_2, \ldots$ (piecewise cubic polynomials with compact support, see De Boor, 1978) in the logarithm of frequency, and the direction-dependence was represented by a Fourier series on a direction interval $3/2$ times wider than the interval of propagation directions in the model. The spatial variation was described by representing each Fourier coefficient by B-splines in the along-shore coordinate y. Actually, all tests carried out so far were with a spatially uniform boundary condition, so $n_y = 1$. The number n_ω of spline coefficients used to represent the frequency dependence was 21. The Fourier series for the directional dependence was cut off after the first order, so $n_\theta = 1$. This only allows for a unimodal directional distribution at each given frequency, but the peak width can be adjusted by the ratio of the zeroth- and first-order coefficients. The reason for choosing almost the full resolution of the model for the frequency dependence and a low resolution for the directional

dependence was that HF radar data, which eventually determine the boundary conditions through inverse modelling (Section 3.1) provide more accurate information about frequency dependence then about directionality.

2.2. HF radar backscatter from the sea surface

Shore-based radar systems employ the ground wave mode of radio propagation where the radar signal is guided by the well-conducting sea surface to follow a path that matches the earth's curvature. Consequently, such systems have the unique capability of providing potentially continuous monitoring of ocean surface conditions over a wide area, out to ranges of up to 200 km from the coast. Operating in the HF band of 3–30 MHz, the transmitted signal interacts strongly with the sea surface and the resulting echo contains a wealth of information about sea surface waves and currents. The physical mechanism responsible for this interaction was first recognised by Crombie (1955) as that of Bragg scattering. Theoretical formulations were derived by Barrick (1972a,b), relating the observed backscatter to the directional spectrum of the sea surface (see also Lipa and Barrick, 1986). In first order, these provide the basis for surface current measurement and systems for making such measurements are now well established. Second-order theory provides the basis for wave measurement.

First-order radar backscatter is related to ocean waves of half the wavelength of the radio signal which propagate toward or away from the antenna, or in other words, to ocean wave components with wavenumber vector equal to $\pm 2\boldsymbol{k}_0$, with $\boldsymbol{k}_0$ as the radar wave vector pointing towards the scattering patch. Transmitting at a frequency of 25.4 MHz, the radio wave length is 11.8 m and the radio waves interact with sea surface waves with a length of 5.9 m and a period of about 2 s. In the absence of currents, the Doppler frequency of the peak is called Bragg frequency, ω_B, and is obtained from the linear dispersion relation (Eqs. (1a) and (1b)) of sea surface waves

$$\omega_B = \pm\sqrt{2gk_0 \tanh(2k_0 d)} \tag{5}$$

with g as the acceleration due to gravity, d the water depth and k_0 the magnitude of $\boldsymbol{k}_0$. In the following, we will assume that all wavenumbers are expressed in a local frame in which the first component of a wavenumber is in the direction of the radar wave vector, so $\boldsymbol{k}_0 = (k_0, 0)$.

Barrick's equation for the first- and second-order radar cross-sections σ^1 and σ^2 can be expressed in terms of dimensionless Doppler frequency $\eta = \omega/\omega_B$ and dimensionless wavenumber $\boldsymbol{K} = \boldsymbol{k}/(2k_0)$ and dimensionless sea surface wave spectrum $Z(\boldsymbol{K}) = (2k_0)^4 S(\boldsymbol{k})$ as (Lipa and Barrick, 1986):

$$\sigma^1(\eta) = 4\pi \sum_{m'=\pm 1} Z(-m'\boldsymbol{K}_0)\,\delta(\eta - m') \tag{6}$$

$$\sigma^2(\eta) = 8\pi \sum_{m,m'=\pm 1} \int_{-\infty}^{\infty}\int_{-\infty}^{\infty} |\gamma_{\eta,D}(\boldsymbol{K},\boldsymbol{K}')|^2 Z(m\boldsymbol{K})\,Z(m'\boldsymbol{K}') \times \delta(\eta - f_{m,m',D}(K,K'))\,\mathrm{d}p\,\mathrm{d}q \tag{7}$$

with $\boldsymbol{K}_0 = (1,0)$ as the dimensionless radar wavenumber,

$$\boldsymbol{K} = \left(p - \frac{1}{2}, q \right) \tag{8a}$$

$$\boldsymbol{K}' = \left(-p - \frac{1}{2}, -q \right) \tag{8b}$$

(so $\boldsymbol{K} + \boldsymbol{K}' = -\boldsymbol{K}_0$), $K = |\boldsymbol{K}|$, $K' = |\boldsymbol{K}'|$,

$$f_{m,m',D}(K,K') = m\sqrt{K \tanh(KD)} + m'\sqrt{K' \tanh(K'D)}\,, \tag{9}$$

$D = 2k_0 d$ the dimensionless depth, and γ a (complex-valued) coupling coefficient consisting of an electromagnetic term (first-order hydrodynamics with second-order Bragg) and a hydrodynamic term (second-order hydrodynamics with first-order Bragg). The first-order spectrum (Eq. (6)) consists of impulse functions at $\eta = -1$ and $\eta = 1$. In reality (see, for example, Fig. 1), these are broadened by current variability and system effects. The integers m and m' define the four second-order sidebands of the Doppler spectrum: m' corresponds to the sign of η, and m to the sign of the difference of η and the normalised frequency of the nearest first-order peak. In computations, Eq. (7) is further simplified to an integral over the direction of $\boldsymbol{K}$ (see Lipa and Barrick, 1986).

Commonly, the *normalised* second-order Doppler spectrum σ_N^2 is predicted, obtained by dividing Eq. (7) by the integral of the nearest first-order peak. This normalisation eliminates effects of system gain and path losses which are not easily accounted for. At Doppler frequencies in the bands $1.1 < |\eta| < 1.4$ and $0.6 < |\eta| < 0.9$, $\boldsymbol{K}'$ is close to $-\boldsymbol{K}_0$. Based on this observation and assuming that the tail of the spectrum falls off with some power p, Hasselmann (1962) proposed the approximation

$$Z(m'\boldsymbol{K}') \approx Z(-m'\boldsymbol{K}_0)(K')^{-p} \tag{10}$$

From Eqs. (2) and (7), the normalised second-order spectrum is now by approximation

$$\sigma_N^2(\eta) = 2 \sum_{m,m'=\pm 1} \int_{-\infty}^{\infty}\int_{-\infty}^{\infty} |\gamma_{\eta,D}(K,K')|^2 Z(m\boldsymbol{K})(K')^{-p} \times \delta\big(\eta - f_{m,m',D}(K,K')\big)\,\mathrm{d}p,q \tag{11}$$

which is linear in the sea surface spectral density. This approximation was employed by Howell and Walsh (1993) to allow application of a wave spectrum retrieval scheme restricted to linear models. In the present study, we could in principle use the normalised nonlinear expression (Eq. (7)) because an iterative retrieval scheme is employed which can handle nonlinear models (Section 3). The approximation (Eq. (11)) was used only to facilitate dealing with the vanishing of spectra produced by the wave model outside the range of wave propagation directions. It avoids possible division by zero in normalising Eq. (7) which would occur if the computed surface wave spectral density in the nearest Bragg wave number is zero. This problem would be particularly serious with wind blowing from the shore. As the wave model does not compute locally generated wind-sea, the computed first-order peak near $\eta = -1$ would be zero, but this is the highest peak in the measurements which has the highest signal-to-noise, and therefore provides most information.

In our software, we chose $p = 6$ in Eqs. (10) and (11), which differs from the value 4 used by, e.g., Howell and Walsh (1993). Our reason of choosing 6 is that the retrieved spectrum represents a first-order wave spectrum, which is the spectrum of free waves satisfying the dispersion relationship (Eqs. (1a) and (1b)). The tail of the first-order spectrum is shorter than the tail of an observed spectrum which contains contributions from free as well as bound waves. For observed spectra, often a k^{-4} dependence is reported. Aziz Tayfun (1990) reported that the corresponding first-order spectrum should have a k^{-6} tail, which we incorporated in the Doppler model approximation, assuming that the wavelength of the wind-sea peak is large enough that Bragg waves (of about 6 m for a 25.4 MHz radar frequency) are indeed in the tail of the spectrum. In fact, we are not totally convinced of the validity of the result by Aziz Tayfun (1990) to describe the spectral tail. However, the retrieval does not appear to be sensitive to the value of p. This was confirmed in a test (on the data of December 21, 1995 at 1400 h described in Section 4) where changing p from 4 to 6 did not significantly alter the outcomes.

In the context of a Doppler model coupled to a wave propagation model, Eq. (11) has the drawback that each half of the second-order spectrum (that is the spectrum in the positive or in the negative Doppler frequency range) is normalised by the integral of the nearest first-order peak. This produces normalised second-order Doppler spectra with both halves having about the same mean level. Rather, we would like to normalise both halves of the spectrum with the *highest* first-order peak to preserve their ratio. This is desirable because the level of the second-order spectrum relative to the noise level determines the accuracy of the observed density, which we can use to design a statistically optimal retrieval (see Section 3). Normalisation of the entire second-order spectrum by the highest first-order peak can be achieved by multiplying the normalised spectrum (Eq. (11)) by the ratio

$$\frac{Z(-m'\boldsymbol{K}_0)}{\max\left(Z(\boldsymbol{K}_0), Z(-\boldsymbol{K}_0)\right)} \tag{12}$$

which can be derived directly from the measured first-order peaks instead of from the computations. As a result, the half of the normalised spectrum corresponding to the highest observed first-order peak is left as it was, whereas the other half is scaled down by the ratio of the lowest to the highest observed first-order peak. Note that by using the ratio (12) from the measurements, the omission of computing locally generated wind-sea in the wave model will not have serious consequences as we do not need to use computed wave spectra in the Bragg wavenumbers for normalisation. The approach is much simpler than the alternative of computing wind-sea spectra in the wave model and reconstructing these as part of the inversion scheme.

3. Inversion method

3.1. Background

Until the present study was undertaken, inversion of HF radar Doppler spectra has always been regarded as a local problem: Doppler spectra corresponding to a single

patch of the sea surface (cell) obtained from two antenna arrays are inverted to an estimate of the local spectrum. The local inversion of HF radar backscatter therefore involves the solution of the integral Eq. (7) or Eq. (11) which in principle at least, provides measurements of the full ocean wave directional spectrum. The has been the subject of much research in this area (see Lipa, 1977, 1978; Wyatt, 1990; Howell and Walsh, 1993; Hisaki, 1996). In the present study, we have developed an inversion scheme which is capable of solving the inversion problem for all measured Doppler spectra simultaneously, assuming that the sea surface spectrum can be regarded as steady (motivated in Section 2.1). The reason is that it allows us to impose physical constraints on the retrieved wave spectra.

The coupled model consisting of a wave propagation model and a radar backscatter model (Section 2) has as input the boundary conditions of the wave model, and as output the normalised second-order Doppler spectra at the measurements cells. To retrieve wave spectra, we try to determine values for the wave model boundary conditions which produce Doppler spectra matching the measured spectra as closely as possible (see Fig. 1). The general approach is as in many data-assimilation schemes developed over the last decade:

- determine a scalar function to express the mismatch between computed and measured spectra;
- express the boundary conditions of the wave model in a suitable manner by some vector of real numbers α, so j is now a function of α (see Section 2.1);
- select and implement a general purpose iterative method for updating α in order to minimise the mismatch j.

Wave spectra at any desired point within the wave model grid can now be computed from the retrieved boundary conditions by one extra model run.

To minimise j, a variant due to Shanno (1978) of the well-known conjugate gradient method (Press et al., 1992) was chosen. It only requires subroutines for the evaluation of j and of its gradient to α

$$\nabla j = (\partial j/\partial \alpha_1, \ldots, \partial j/\partial \alpha_m) \tag{13}$$

at an arbitrary value of α. The subroutine for evaluating j runs the coupled model and then evaluates the cost function based on the measured and computed Doppler spectra. The subroutine for evaluating ∇j applies the chain rule of differentiation to compute the gradient of j to the variables which are present at each stage of the computation of j. It does this in reverse order; each routine in the forward model has its counterpart, or *adjoint*, in the gradient computation.

3.2. Criterion for mismatch

The criterion for mismatch was derived from the *likelihood function* of the observations $p(\sigma_N^{2,\mathrm{obs}}|\sigma_N^{2,\mathrm{pre}})$ which is the conditional probability density of the observed normalised second-order Doppler spectral density $\sigma_N^{2,\mathrm{obs}}$, given the predicted spectral density $\sigma_N^{2,\mathrm{pre}}$ based on the models of Section 2. The observed spectral density is the mean square of the magnitudes of Fourier transforms of the Doppler return signals

within a particular frequency band. These Fourier transforms are by approximation complex Gaussian, due to the central limit theorem (Brillinger, 1975). Therefore, from (Mastenbroek and de Valk, 1998; Eq. (A2)) we find that

$$p\left(\sigma_N^{2,\mathrm{obs}} | \sigma_N^{2,\mathrm{pre}}\right) = c\left(\sigma_N^{2,\mathrm{obs}}, \upsilon\right) f^{-\upsilon} \exp(-\upsilon/f) \tag{14a}$$

with f the ratio of predicted to measured spectral density, υ the number of degrees of freedom of the spectral estimate and $c(\sigma_N^{2,\mathrm{obs}}, \upsilon)$ a factor which does not depend on the predicted spectral density. We assume that in addition to the predicted signal, a white noise is present with a level depending on cell and antenna. This level is estimated from the observed spectral densities in the highest and lowest Doppler frequencies where no other signal is assumed to be present. Therefore,

$$f = \frac{n + \sigma_N^{2,\mathrm{pre}}}{\sigma_N^{2,\mathrm{obs}}} \tag{14b}$$

in Eq. (14a). Spectral densities are measured for various Doppler frequencies, for various cells and for one or two antenna arrays, depending on the configuration used. We will simply label them with an index i which represents a combination of frequency, cell and antenna. A high value of the likelihood function corresponds to a close match, so a criterion for mismatch is

$$\sum_{i=1,\ldots,n} -\log\ p\left(\sigma_N^{2,\mathrm{obs}}(i) | \sigma_N^{2,\mathrm{pre}}(i)\right) \tag{15}$$

as maximising the likelihood is equivalent to minimising the negative of its logarithm. Inserting Eq. (14a) into Eq. (15) and ignoring terms which do not depend on the predicted spectral density, we obtain the mismatch

$$j^{\mathrm{ML}} = \sum_{i=1,\ldots,n} \upsilon_i \left[1/f(i) + \log f(i) - 1\right] \tag{16}$$

with the term -1 added in order to make the minimum of the mismatch for each single bin equal to zero (it is irrelevant to the solution). υ_i was equal for all i so it had no influence on the outcomes of the retrieval.

If the Doppler spectral measurements for different frequency bins, cells and antennae were independent, then minimising the mismatch j^{ML} would be equivalent to maximum likelihood estimation, a common procedure in statistical inference. Independence does not completely hold; e.g., spectra corresponding to different cells are dependent due to beamforming. This dependence does not invalidate the estimator; the only consequence is that estimates are somewhat less accurate than they would be if independent.

The mismatch (Eq. (16)) for a single i is plotted in Fig. 3 as a function of the ratio of predicted to measured spectral density f (drawn line). Using Eq. (16), often rather high predicted Doppler spectra were found in comparison with measured spectra. This may be related to the asymmetry of the mismatch, which penalises a low spectral ratio f more than a high one (see Fig. 3). To suppress high ratios somewhat more, a

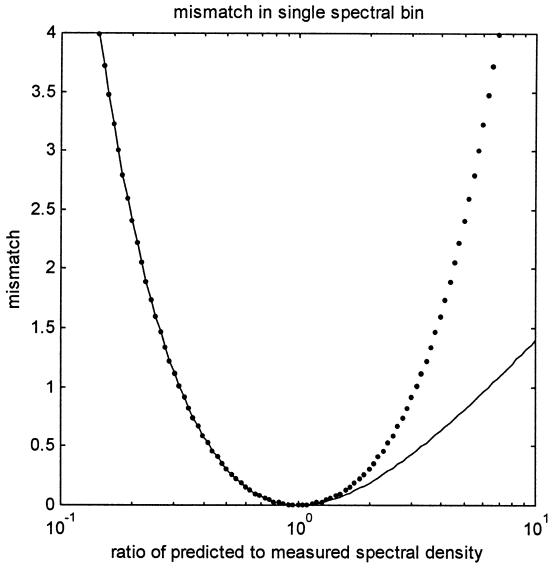

Fig. 3. Criteria for the mismatch between computed and measured radar Doppler spectra as a function of the ratio f of predicted to measured spectral density (Eq. (14b)). Drawn: function j^{ML} (Eq. (16)) from the log-likelihood function. Dotted: modified mismatch j (Eq. (17)) applied in this study.

modification of Eq. (16) was introduced, making it symmetric as a function of the logarithm of f:

$$j = \max\left(j^{\mathrm{ML}}, j^{\mathrm{RE}}\right) \tag{17}$$

with

$$j^{\mathrm{RE}} = \sum_{i=1,\ldots,n} v_i\left[f(i) - \log f(i) - 1\right]. \tag{18}$$

The modified mismatch function j as a function of f is the dotted line in Fig. 3. Note that it penalises high values of f more severely than j^{ML}, although less severely than a sum of squares type mismatch function proportional to $|n(i) + \sigma_N^{2,\mathrm{pre}}(i) - \sigma_N^{2,\mathrm{obs}}(i)|^{-}$. Some experimentation showed that replacing j^{ML} by j generally improved results. Spectral densities were not included in the mismatch in bins where the signal-to-noise ratio of the measurements was below 10. Also bins surrounding the lowest of the two first-order peaks were ignored if the energy of the lowest peak was less than half of the energy of the highest peak. Finally, only densities at relative frequencies in the bands $1.1 < |\eta| < 1.4$ and $0.6 < |\eta| < 0.9$ were used, as the linearised Doppler model is only valid in this range (see Section 2.2).

3.3. Tests of the inversion scheme on simulated data

To examine the sensitivity of the wave spectrum retrieval scheme to various parameters, a limited set of tests was performed. The procedure was as follows. First, a

simulated wave boundary condition was chosen. Using the coupled wave propagation/radar backscatter model, Doppler spectra for a number of selected cells were computed. These data were then inserted into the retrieval scheme as if they were measurements to estimate the boundary conditions of the wave model. The retrieved boundary conditions were then compared with the ones used originally to simulate the data. The only difference between the models used to simulate data and the models used in the retrieval was that the former also allowed for the addition of locally generated wind-sea. In the context of these tests, wind-sea means wave energy which has not been propagated from the boundary, and which may therefore not be retrievable by adjusting boundary conditions. It also affects the ratio (12) which is used to normalise the data (see Section 2.2). An example configuration of seabed bathymetry, HF radar measurement cells and antennae is shown in Fig. 4.

The outcome of the retrieval depends on many parameters of which we mention the number of cells used, antenna arrays used (''Master'', ''Slave'', or both), offshore wave conditions and spatial variability in offshore wave conditions, noise level in observed Doppler spectra, bathymetry, etc. This leads to a large number of alternatives from which we have selected a few given in Table 1.

Swell with a period of 10 s is obliquely incident with respect to the coast normal, and wind-sea with a period of about 5 s propagates from the other quadrant. In one test, a shoal is present (see also Fig. 4) which causes waves to refract, resulting in a wave field

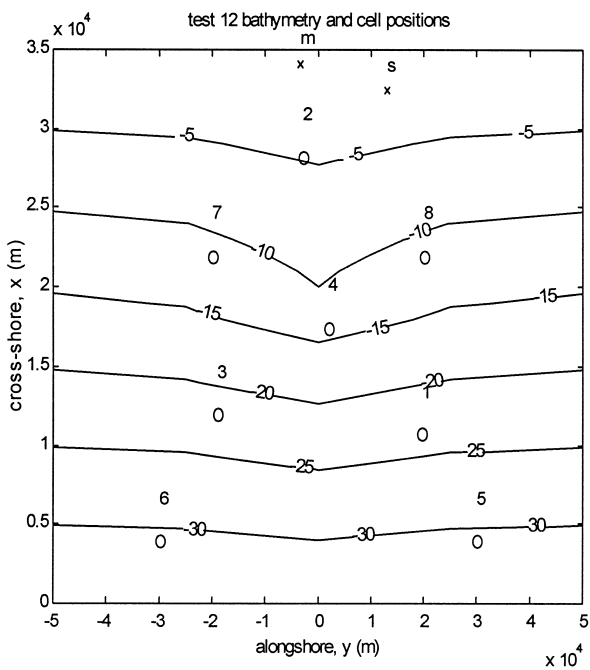

Fig. 4. Example of test layout. Contour lines of bathymetry, positions of radar (×) and cell positions (o).

Table 1
Test conditions and results: M = ''master'', S = ''slave'', θ = wave direction relative to coast normal, H_{m0} = significant wave height. See Fig. 4 for cell and antenna positions

Test	Cells	Antennae	Swell		Wind-sea		Seabed	Performance	
			θ	H_{m0}	θ	H_{m0}		err θ	err S
1	1–2	M and S	40°	1 m	–	0	plane	2°	11%
2	1–2	S	40°	1 m	–	0	plane	2°	11%
3	1–2	M	40°	1 m	–	0	plane	5°	29%
4	1–4	M	40°	1 m	–	0	plane	2°	17%
5	1–8	M	40°	1 m	–	0	plane	2°	6%
6	1–8	M	40°	1 m	0°	$\ll$ 1 m	plane	1°	6%
7	1–8	M	40°	1 m	20°	1 m	plane	2°	12%
8	1–8	M	40°	1 m	−20°	1 m	plane	2°	13%
9	1–8	M	40°	1 m	−40°	1 m	plane	2°	15%
10	1–8	M	40°	1 m	−60°	1 m	plane	2°	18%
11	1–8	M	40°	1 m	–	0	shoal	1°	6%

which varies also in along-shore direction. The observed Doppler spectra are given at some or all of the cell positions indicated in Fig. 4, labelled from 1 to 8. In tests with a single radar antenna, data with varying numbers of cells were used to test the capability of the retrieval scheme to distinguish waves from different directions using a single radar. The spatial dimensions of the grid roughly correspond to the configuration of the Holderness experiment (see Section 4).

To compare the performance of the retrieval scheme in different test cases, the following criteria were defined: a normalised error in the predicted non-directional wave spectrum and a normalised density-weighted error in the mean propagation direction

$$\text{err } S = \frac{\int |\hat{S} - S| \mathrm{d}\,\omega}{\int S \mathrm{d}\,\omega} \quad \text{err } \theta = \frac{\int S |\hat{\theta} - \theta| \mathrm{d}\,\omega}{\int S \mathrm{d}\,\omega} \tag{19}$$

where $\hat{S}$ and $\hat{\theta}$ are the retrieved values of the non-directional spectral density S and the frequency-dependent mean wave direction θ, respectively. Note that err S reflects errors in the heights as well as in the periods of spectral peaks. The results for the various tests are listed in the last two columns of Table 1.

They show that using a single radar in combination with Doppler spectrum data from only two cells, already a fair estimate of the wave boundary conditions can be obtained (compare tests 1, 2 and 3). The result with a single antenna, however, depends strongly on the viewing angle relative to the direction of wave propagation (compare tests 2 and 3). Increasing the number of cells to four and eight results in a better match with the simulated wave spectra (tests 4 and 5). Adding a little wind sea in test 6 gives similar results for the energy density spectrum but improves the retrieval of wave directions significantly, possibly because the ratio (12) of the simulated data is altered. Increasing the wind sea to a height comparable to that of the swell waves in test 7 affects the results obtained for the spectral density negatively. In the retrieval, it should be possible

to approximate this wind sea with a direction of 20° from the coast normal by inserting it as swell at the boundary. Therefore, the reduced performance with increased the wind sea is probably due to a problem in distinguishing the two peaks from the data. The retrieved directions remain accurate, however, also when increasing the angle of incidence with respect to the coast normal (tests 8–10). Apparently, as swell and wind-sea do not overlap in frequency, the assumption of (frequency-dependent) unimodal directional distributions at the boundary is not a limitation (Section 2.1). The largest error in the spectral density is obtained in test 10, possibly because the wind-sea of direction 60° is difficult to match by modifying boundary conditions. Finally, in test 11, the presence of a shoal has no negative consequences for the retrieval of the offshore wave boundary conditions.

4. Application to HF radar data from Holderness

Test results with simulated data gave enough confidence to attempt application of the retrieval method to HF radar data. The data were collected by the University of Sheffield at the Holderness coast in the winter of 1995–1996. They used the OSCR HF radar system of Fugro GEOS, which consists of two linear arrays and operates at a frequency of 25.4 MHz. Fig. 5 shows the configuration of antenna arrays and cells as well as some depth contours. Depth ranges from 11 to 54 m within the area covered by the cells in Fig. 5.

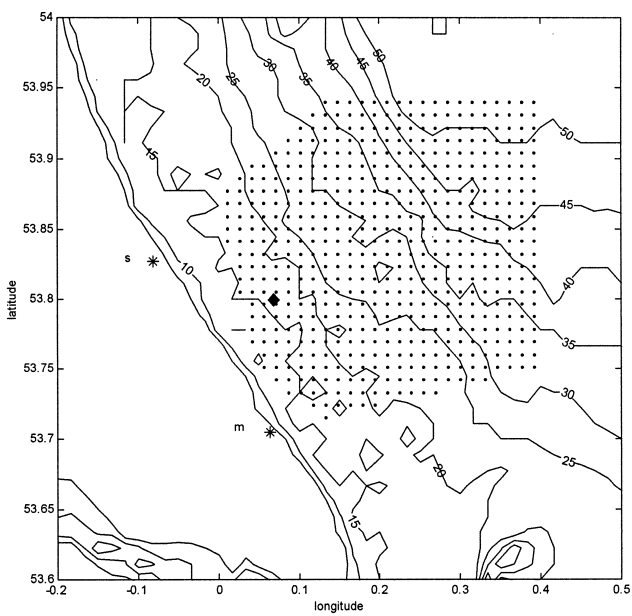

Fig. 5. Holderness depth contours (values in meters below chart datum), HF radar antenna positions (stars) and measurement cells (dots). ‘‘s’’: slave array. ‘‘m’’: master array. Black diamond: location of wave buoy.

Fig. 6 shows the grid of the wave model used in the retrieval of wave spectra from the Holderness HF radar data. It also shows the antenna positions. The model grid extends much further along the coast than the measurement cells, in order to allow obliquely incoming waves to propagate from the offshore boundary of the model to the measurement cells. Note that the cells are all located offshore the stretch of coast between the antenna arrays. Potentially, Doppler spectra could have been gathered over a much larger area. However, as the Holderness experiment was designed with cell-by-cell retrieval from data of both arrays in mind, these other data were not stored. The restricted coverage is a drawback when applying the coupled retrieval method on data of a single antenna array, because it limits the range of angles from which waves can be observed and therefore also limits the information about wave directionality which is available using a single antenna.

On December 21, 1995 at 1400 h, a wave buoy deployed in the same area (see Fig. 5) indicated swell from NNE with a peak period of about 11 s, and wind-sea from SE with a peak period of about 5 s. Fig. 7 shows (non-directional) wave spectra and mean wave directions measured by the wave buoy and retrieved from the HF radar data using the coupled wave propagation/radar scattering model at a cell close to the buoy location. Results are shown based on data from both antennae, data from the slave only, and data from the master only, respectively. Fig. 1 shows an example of measured Doppler spectra and Doppler spectra computed from wave spectra retrieved from data of the slave array (left) and the master array (right) at the same cell.

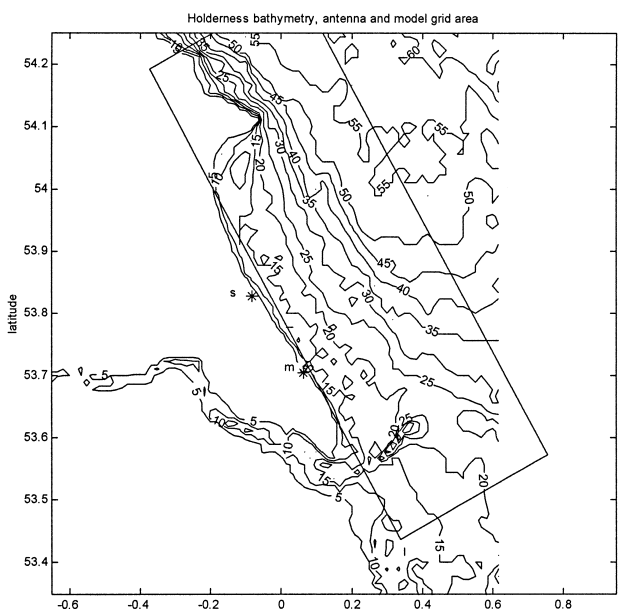

Fig. 6. Holderness depth contours (values in metres below chart datum), HF radar antenna positions (stars) and area covered by wave model grid. ‘‘s’’: slave array. ‘‘m’’: master array.

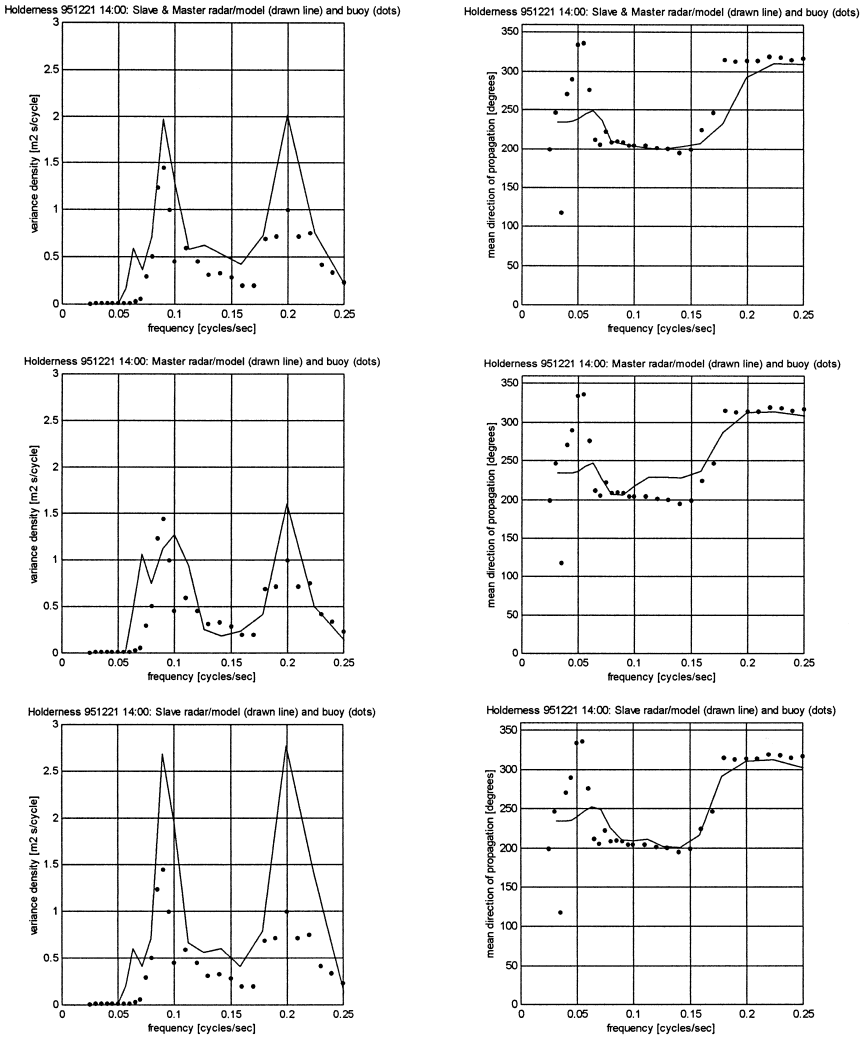

Fig. 7. Wave spectra on December 21, 1995 at 1400 h retrieved from HF radar data/model (line) and from buoy data (dots). Retrieved spectra are based on HF radar data from (a) both arrays, (b) master only, and (c) slave only. Left: omnidirectional spectral density; right: mean propagation direction.

Overall, the results with all three antenna configurations in Fig. 7 are similar. The variance is somewhat too high using the slave array only, but directions are better than when using the master array or when using both arrays. The retrieval of the wind-sea peak is surprisingly good in view of the fact that the scheme was not intended for wind-sea retrieval. Apparently, it has adjusted boundary conditions to match peaks in Doppler spectra related to the wind-sea as closely as possible. This is possible because the wind-sea is propagating into the grid domain of the model from the offshore

boundary. The only error we have made is that local growth is neglected, which was estimated to be of minor significance.

Fig. 8 shows mean propagation directions in three spectral bands retrieved from the slave array on the gridcells shown in Fig. 5 (the coast is to the southwest of the vectors shown). For each separate band, little spatial variability of the mean direction is seen; only swell waves in the band of 0.0–0.1 Hz are seen to refract over up to about 30°. The lack of variability of the wave direction seems in contrast with results from cell-by-cell inversion of the same data shown in (Wyatt, 1998; Fig. 8). These results seem to indicate that waves from the north are turning toward the coast in the band of 0.1–0.2 Hz. The explanation is that this band contains an approximately equal mixture of swell and wind-sea with completely different directions, as Fig. 7 shows. The effect on the mean direction obtained from the coupled retrieval scheme is seen in Fig. 8, which is somewhere in between the directions of swell (dominant in the band of 0.0–0.1 Hz) and wind-sea (dominant in the band 0.2–0.3 Hz). Coupled retrieval assumes a spatially uniform wave spectrum offshore. Therefore, it gives a rather uniform ratio of wind-sea and swell in 0.1–0.2 Hz and equally uniform mean direction. In cell-by-cell inversion, the relative magnitudes of sea and swell in this band may vary more, leading to a spatially more variable mean wave direction. The variation in wave direction by Wyatt (1998) is therefore only for a minor part due to refraction and rather seems to reflect that in the 0.1–0.2 Hz band swell dominates somewhat in the north and wind-sea in the south of the area covered by the cells in Fig. 5. It would be interesting to see whether the coupled retrieval method could produce similar results if the boundary conditions were allowed to vary along the offshore boundary.

Another result is shown in Fig. 9 for data collected at January 1, 1996 at 2000 h. In this example, the match between the buoy spectrum and the spectra retrieved from two arrays, the master array only, and the slave array only is very close in all cases. This is a typical wind-sea situation but it can be retrieved very well by representing the waves entirely as generated at open sea and travelling into the wave model grid through its offshore boundary. It must be noted that such wind-sea retrieval is not possible if the wind is blowing from the shore as the wave model does not incorporate local growth; however, in most applications, such relatively low and short waves which do not affect the coast are not of interest. Still, it may be worthwhile to extend the range of propagation directions of the model to the full circle for applications in areas with irregularly varying coastlines and bathymetry.

Table 2 summarises the values of the performance criteria used in Section 3.3 obtained in the Holderness applications discussed above. These criteria are strict: a 50% overestimate of significant wave height with a correct spectral shape gives err $S = 125\%$. Clearly, the errors are an order of magnitude larger than those obtained with simulated data (see Table 1). Sampling variability and probably other deviations of our models from reality determine the quality of the results.

So far, not much attention has been paid to the computational efficiency of the method. The applications to data of Holderness took about 2 h per data-set on a personal computer with 267 MHz Pentium 2 processor with 128 Mb RAM. The computational load was mostly due to the application of the Doppler model to 559 cells and two antenna arrays, even though integration contours and integrands were computed once

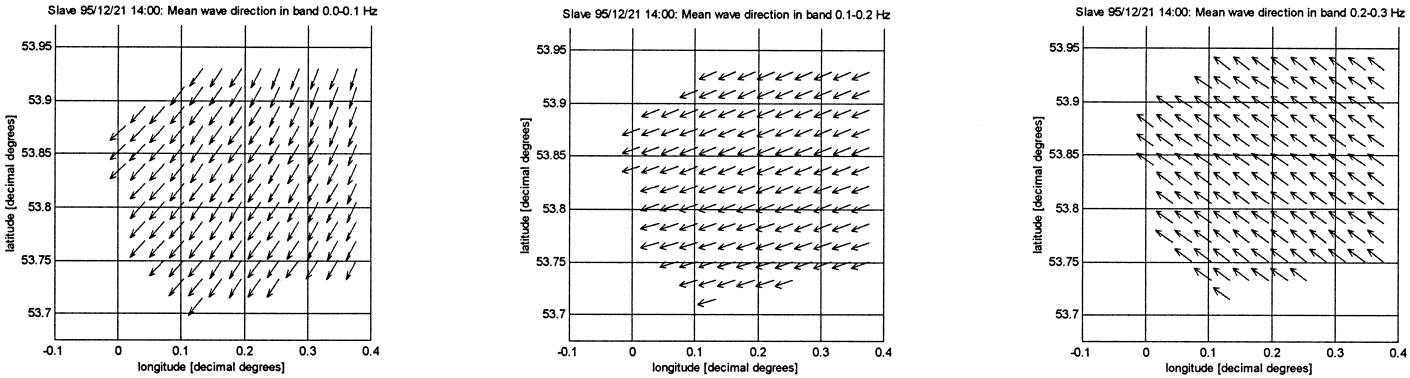

Fig. 8. Mean propagation directions on December 21, 1995 at 1400 h in three frequency bands as retrieved from HF radar data/model using the slave array only. Bands are 0.0–0.1 Hz (left), 0.1–0.2 Hz (middle) and 0.2–0.3 Hz (right).

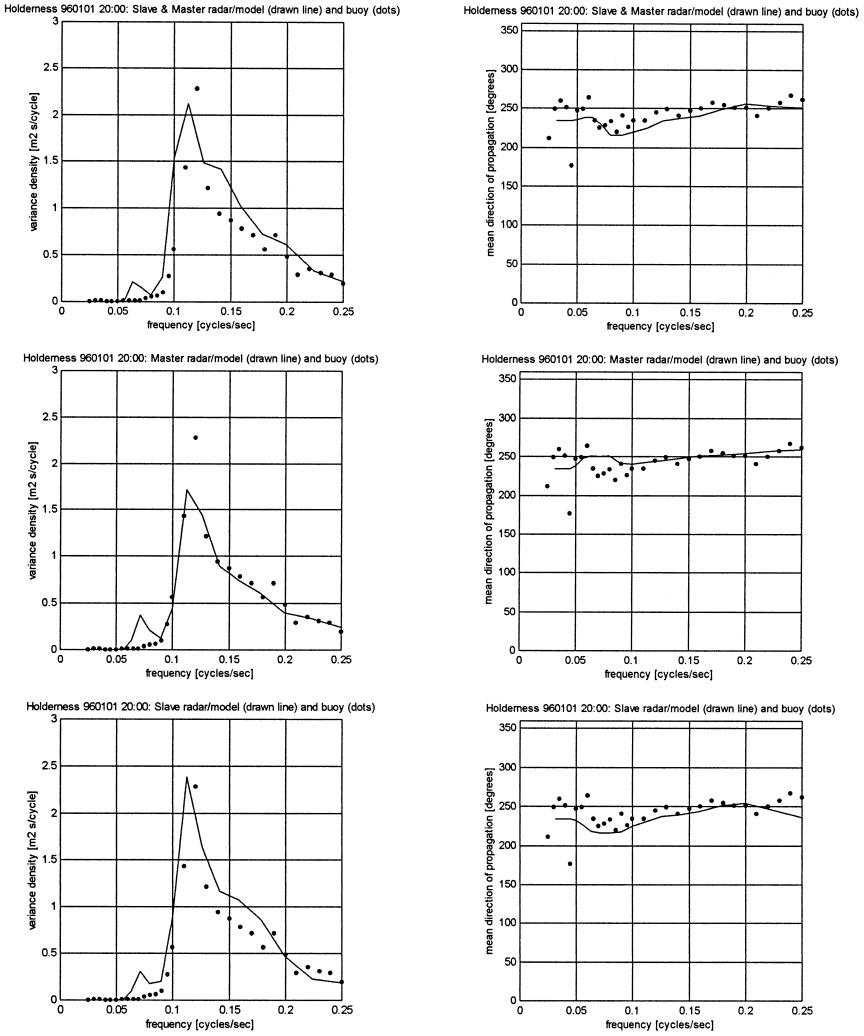

Fig. 9. Wave spectra retrieved from HF radar data/model (line) and from buoy data (dots) on January 1, 1996 at 2000 h. Retrieved spectra are based on HF radar data from (a) both arrays, (b) master only and (c) slave only. Left: omnidirectional spectral density; right: mean propagation direction.

and then stored for subsequent iterations. However, also more iterations were needed to reach a stable solution than in the tests with simulated data (Section 3.3). The latter is probably related to the presence of noise in the Holderness data which reduces the sensitivity of the misfit (Section 3.2) to the wave model boundary conditions. Tests with different starting values for the boundary conditions showed that local minima of the misfit were not causing this problem, as all runs eventually lead to approximately the same solution. Therefore, the problem may be due to poor condition (a large spread in

Table 2
Holderness performance according to the criteria (Eq. (19)); M = ''master'', S = ''slave''. Buoy spectra were regarded as ''truth''

Date/time	December 21, 1995 at 1400 h			January 1, 1996 at 2000 h		
Antennae	M	S	M and S	M	S	M and S
err θ	11°	7°	15°	10°	7°	10°
err S	49%	125%	72%	15%	30%	35%

the eigenvalues of the Hessian of the misfit function) and may be solved by preconditioning (see Press et al., 1992). The algorithm may also be speeded up by reducing the number of cells, as the data from the 559 cells are not fully independent anyway.

5. Conclusions

A new scheme for retrieval of wave spectra in coastal seas from HF radar data has been developed which is capable of measuring directional wave spectra even from the data of the single antenna array. It does this by making use of a wave propagation model to link wave spectra, and therefore also HF radar Doppler spectra at different points in space. The resulting scheme processes all HF radar data within the area covered by the system simultaneously. In coastal applications, the method offers increased flexibility in the radar configuration and improved coverage.

Generally, retrieved wave spectra are somewhat too high; however, this can be easily improved by modifying the criterion used to measure the mismatch between observed and predicted Doppler spectra in Section 3.2.

In the applications to data collected at the Holderness coast, wind-sea propagating toward the shore can be retrieved rather well by representing these waves entirely as generated at open sea and estimating the offshore boundary condition of the wave model.

Tests were carried out comparing wave spectra retrieved from data of both antenna arrays and from a single array. It is not possible to claim that the results based on two arrays are substantially better than with a single array. This shows that the new retrieval method is indeed capable of measuring directional wave spectra from the data of a single HF radar antenna array. It must be noted that we could not use the full potential of the idea because HF radar data covering only a limited area were available in this study.

In the future, the coupled wave retrieval scheme may be further explored and improved by

- using the full radar coverage possible;
- including wave–current interaction in the model estimating the current field from surface current data provided by the HF radar system itself, and testing this in an area where the interaction is strong;

- retrieval of not only boundary conditions but also, e.g., constants determining the rate of dissipation;
- including spatial variability of offshore wave conditions;
- extending the range of propagation directions of the wave model and generalising the propagation scheme to deal with more complex shapes of coastlines and depth contours;
- possibly also retrieval of the locally generated wind-sea, although this is likely to be of less interest for most applications;
- applications with longer radar wavelengths and as a consequence, a larger area of sea covered by the HF radar system.

Acknowledgements

The authors would like to thank Dr. Lucy Wyatt of the Sheffield Centre for Earth Observation Science, University of Sheffield for her support. This study was partly funded by the EC MAST programme as part of the SCAWVEX project (MAS2CT940103).

References

Aziz Tayfun, M., 1990. High wave number/frequency attenuation of wind-wave spectra. J. Waterw. Port Coastal Ocean Eng. 116, 381–398.

Barrick, D.E., 1972a. First-order theory and analysis of MF/HF/VHF scatter form the sea. IEEE Trans. AP/20, 2–10.

Barrick, D.E., 1972. Remote sensing of sea state by radar. In: Derr, V.E. (Eds.), Remote sensing of the Troposphere, Boulder, CO, NOAA, Environmental Research Laboratories, pp. 12.1–12.46.

Booij, N., Holthuijsen, L.H., Ris, R.C., 1996. The SWAN wave model for shallow water. Proc. 25th Int. Conf. Coastal Eng., Vol. 1, Orlando, USA, pp. 668–676.

Brillinger, D.R. (1975), Time Series — Data Analysis and Theory. Holt, Rinehart and Winston.

Crombie, D.D., 1955. Doppler spectrum of sea echo at 13.56 Mc/s. Nature 175, 681–682.

De Boor, C., 1978. A Practical Guide to Splines. Springer-Verlag, New York.

Hasselmann, K., 1962. Determination of ocean wave spectra from Doppler radar return from the sea surface. Nat. Phys. Sci. 229, 16–17.

Hisaki, Y., 1996. Nonlinear inversion of the integral equation to estimate ocean wave spectra from HF radar. Radio Sci. 31, 25–39.

Howell, R., Walsh, J., 1993. Measurement of ocean wave spectra using narrow-beam HF radar. IEEE J. Oceanic Eng. 18, 296–305.

Komen, G.J., Cavaleri, L., Donelan, M., Hasselmann, K., Hasselmann, S., Janssen, P.A.E.M. (Eds.) 1994. Dynamics and Modelling of Ocean Waves. Cambridge Univ. Press.

Ledgard, L.J., Wyatt, L.R, 1997. Measurement of Ocean Waves Using the OSCR HF Radar System. Final Report to NERC, University of Sheffield.

Lipa, B.J., 1977. Derivation of directional ocean-wave spectra by integral inversion of second-order radar echoes. Radio Sci. 12, 425–434.

Lipa, B.J., 1978. Inversion of second-order radar echoes from the sea. J. Geophys. Res. 83, 959–962.

Lipa, B.J., Barrick, D.E., 1986. Extraction of sea state from HF radar sea echo: mathematical theory and modelling. Radio Sci. 21 (1), 81–100.

Mastenbroek, C., de Valk, C.F., 1998. A semi-parametric algorithm to retrieve ocean wave spectra from SAR. Manuscript, submitted to J. Geophys. Res.

Mei, C.C., 1989. The applied dynamics of ocean surface waves. World Scientific, Singapore.

Petit, H., 1995. Note on the discretization of the propagation of wave action in PHIDIAS. Technical note, WL|Delft Hydraulics, Delft.

Press, W.H., Teukolski, S.A., Vetterling, W.T., Flannery, B.P., 1992. Numerical Recipes in FORTRAN: the Art of Scientific Computing. Cambridge Univ. Press, Cambridge.

Shanno, D.F., 1978. Conjugate gradient methods with inexact searches. Math. Oper. Res. 3, 244–256.

Wyatt, L.R., 1990. A relaxation method for integral inversion applied to HF radar measurement of the ocean wave directional spectra. Int. J. Remote Sens. 11, 1481–1494.

Wyatt, L.R., 1997. An example of wave variability during the Holderness 2 experiment. SCAWVEX technical report 16, Sheffield Centre for Earth Observations Science, University of Sheffield, Sheffield.

Wyatt, L.R., 1998. Variability in wave spectra measured by HF radar. In: Edge, B.L. Helmsley, J.M. (Eds.), Ocean Wave Measurement and Analysis, Vol. 1, Proceedings of the 3rd International Symposium, Waves97, pp. 355–369.

Wyatt, L.R., Thompson S.P., Burton, R.R., 1998. Evaluation of HF radar measurement, Coastal Eng. (this issue).